

Enhancement of associated $H^\pm W^\mp$ production in the NMSSM

R. Enberg,^{1,*} R. Pasechnik,^{2,†} and O. Stål^{3,‡}

¹*Department of Physics and Astronomy,
Uppsala University, Box 516, SE-751 20 Uppsala, Sweden*

²*Department of Astronomy and Theoretical Physics,
Lund University, SE-223 62 Lund, Sweden*

³*Deutsches Elektronen-Synchrotron DESY,
Notkestraße 85, D-22607 Hamburg, Germany*

Abstract

We study the associated production of a charged Higgs and a W boson in high-energy pp collisions at the Large Hadron Collider. This is an interesting process for charged Higgs discovery, or exclusion, since the production cross section could depend strongly on the model, offering potential discriminating power between supersymmetric extensions of the Standard Model with minimal or extended Higgs sectors. We compute the cross section for this process in the next-to-minimal supersymmetric Standard Model (NMSSM), at the tree level for quark-quark scattering and at one-loop level for gluon-gluon scattering. The most important corrections beyond leading order are taken into account using an improved Born approximation. We find that the $pp \rightarrow H^\pm W^\mp$ cross section can be resonantly enhanced by up to an order of magnitude over its MSSM value (both for $\sqrt{s} = 7$ TeV and 14 TeV) through the contributions of heavy, neutral, singlet-dominated Higgs bosons appearing in the s -channel. Since such Higgs mass configurations are normally not possible in the MSSM, the observation of associated $H^\pm W^\mp$ production at the LHC could provide a striking, although indirect, signature of a more complicated Higgs sector.

* Rikard.Enberg@physics.uu.se

† Roman.Pasechnik@thep.lu.se

‡ oscar.stal@desy.de

I. INTRODUCTION

There are good phenomenological and theoretical reasons to consider supersymmetric (SUSY) extensions of the Standard Model, including amelioration of the hierarchy problem or the fine-tuning of the Higgs mass, unification of the gauge couplings, and the existence of a dark matter WIMP candidate. The most common SUSY model is the minimal supersymmetric extension of the Standard Model (MSSM) [1, 2], which exhibits all of the above benefits. These benefits come at the price of introducing a mass term (called the μ -term) for the two Higgs doublets that are required in the MSSM. This leads to another fine-tuning problem, namely why the mass parameter μ of the Higgs doublets should be at the electroweak mass scale, as is required by phenomenology. This is known as the μ -problem. Furthermore, the mass of the lightest Higgs boson cannot be less than ~ 115 GeV, while in the MSSM at the tree-level it has an upper limit equal to the Z boson mass. To fulfill the experimental constraints, large corrections to the Higgs mass from top- and stop-loops are needed, which require a rather large stop mass leading to an additional amount of fine-tuning in the model. If we take fine-tuning arguments seriously, we may therefore consider whether there are alternatives to the MSSM (see e.g. [3, 4]).

One such alternative is the next-to-minimal supersymmetric Standard Model (NMSSM), which has recently been reviewed in Refs. [5, 6]. In the NMSSM, there is in addition to the two Higgs doublets of the MSSM a singlet Higgs field, which is the scalar component of a chiral singlet superfield added to the MSSM superpotential. The reason for introducing this additional scalar is that the μ -term is now dynamically generated, so that the fine-tuned parameter μ is no longer needed. This scalar mixes with the other scalars from the two doublets, leading to a Higgs sector with seven Higgs bosons, compared to the five present in the MSSM. The fermion component of the singlet superfield, the singlino, additionally mixes with the neutralinos, providing interesting possibilities for dark matter that can be, e.g., singlino or singlino–Higgsino-dominated [5], or very light [7, 8].

There are two extra neutral Higgs bosons in the NMSSM compared to the MSSM; one CP-even and one CP-odd. The tree-level mass relations for the Higgs bosons are then also modified, and it is possible for one or more Higgs bosons to be quite light. In particular the lightest CP-odd Higgs, A_1 , can be significantly lighter than in the MSSM—viable scenarios with $m_{A_1} < 2m_b$ exist [9]. The charged Higgs boson can also be rather light [10, 11], albeit not as light as the A_1 .

Because of the different Higgs phenomenology due to the modified mass relations and the additional particles, the parameters of the model are not as constrained as in the MSSM, and new decay channels and production mechanisms may become important at the LHC. For example, the charged Higgs may decay as $H^+ \rightarrow W^+ A_1$, and the A_1 in turn may decay dominantly as $A_1 \rightarrow b\bar{b}, \tau^+ \tau^-$. Such differences are important to take into account in searches at LHC, so that no possibilities are missed.

In this paper, our focus is on production of the charged Higgs boson H^\pm in association with a W^\mp boson. This is not the main production channel usually considered for H^\pm and, to the best of our knowledge, it has not been studied in the context of the NMSSM. It was however pointed out in Ref. [12] that a related process, the associated central exclusive production of $H^\pm W^\mp$, may be useful in the NMSSM.

The usual production mechanisms for H^\pm are top quark decays $t \rightarrow H^+ b$ for light charged Higgs (where the charged Higgs boson mass $m_{H^\pm} < m_t$), and production with a top, $bg \rightarrow H^- t$ or $gg \rightarrow H^- t\bar{b}$, for heavy charged Higgs ($m_{H^\pm} > m_t$). The associated pro-

duction mechanism may, however, be important to secure additional information about the Higgs sector if the charged Higgs is first observed in one of the above-mentioned processes. An advantage of the $H^\pm W^\mp$ process is that a leptonically decaying W may be used as an experimental requirement. The cross section for associated production is as we shall see rather model-dependent, and the observation of this process may therefore provide constraints on the model parameters. For example, in the NMSSM, smaller $\tan\beta$ is allowed, leading to a possible enhancement of the cross section. A potentially more important difference between the MSSM results and the NMSSM comes from the resonant s -channel exchanges of additional singlet-dominated Higgs bosons. Due to the very restricted mass relations of the MSSM Higgs sector, these contributions cannot be resonant in the MSSM, while in the NMSSM they can. The resonant enhancement of the parton-level cross section will also enhance the hadron-level cross section in some range of charged Higgs boson masses and this enhancement could be potentially visible at the LHC. It could be important for discerning differences between MSSM and NMSSM, and for setting limits on the parameter space.

The $H^\pm W^\mp$ production channel was first considered in [13], where the cross sections were calculated in the approximation that $m_b = 0$. This study did not include any contribution from squark loops. The cross sections were later calculated in full generality for two-Higgs-doublet models (2HDM) and the MSSM in [14–17], where in particular [16, 17] included the squark loop contributions. In [18], it was further shown that there may be a substantial enhancement of the cross section compared to the MSSM in a general 2HDM. Our paper extends these studies to the NMSSM, and we are going to investigate in particular the differences between the MSSM and the NMSSM for this process.

Next-to-leading order (NLO) corrections to the $b\bar{b} \rightarrow H^\pm W^\mp$ subprocess, including QCD, SUSY QCD, and electroweak contributions, are known for the MSSM [19–24]. There have also been phenomenological studies of this process for the LHC at 14 TeV [22, 25–28]. While we do discuss the LHC aspects of the $H^\pm W^\mp$ process in the NMSSM below, the inclusion of NLO corrections and a detailed study of LHC signatures are beyond the scope of this paper and will be left for future studies.

Finally, we restrict ourselves to the case of charged Higgs bosons heavier than the top quark, which means that the $t \rightarrow bH^+$ production mechanism is not effective. The reason is twofold: first, this decay is the same in the MSSM and the NMSSM, but we are interested in differences between the two models. Second, the experimental constraints on this decay channel are already quite strict [29–31], ruling out $\text{BR}(t \rightarrow bH^+) > 5 - 10\%$ (in the MSSM).

II. THE NMSSM HIGGS SECTOR

The NMSSM is defined by removing the μ -term from the MSSM superpotential and adding a singlet chiral superfield \hat{S} , which only couples to the Higgs doublets. Assuming scale invariance, the general form of the superpotential is

$$W_{\text{NMSSM}} = W_{\text{MSSM}} + \lambda \hat{S} \hat{H}_u \hat{H}_d + \frac{\kappa}{3} \hat{S}^3. \quad (2.1)$$

In the above superpotential, the (unchanged) Yukawa terms are contained in W_{MSSM} . The scalar potential of the NMSSM is obtained from the F - and D -terms plus the soft SUSY-breaking terms for the Higgs sector,

$$V_{\text{soft}} = m_{H_u}^2 |H_u|^2 + m_{H_d}^2 |H_d|^2 + m_S^2 |S|^2 + \left[\lambda A_\lambda S H_u H_d + \frac{1}{3} \kappa A_\kappa S^3 + \text{h.c.} \right], \quad (2.2)$$

where the dimensionless couplings λ and κ , the soft SUSY-breaking parameters A_λ and A_κ with dimension of mass, and the singlet mass m_S are new parameters compared to the MSSM. As usual, m_S is fixed by the minimization of the potential. Requiring that S acquires a vacuum expectation value (vev), $s = \langle S \rangle$, yields an additional new parameter of the model, and gives rise to an effective μ -parameter $\mu_{\text{eff}} = \lambda s$. Together with the ratio of vevs of the two Higgs doublets, $\tan \beta = v_u/v_d$, where $v_u^2 + v_d^2 = v^2 = (174 \text{ GeV})^2$, we have six free parameters of the Higgs sector of the NMSSM: $\lambda, \kappa, A_\lambda, A_\kappa, s$, and $\tan \beta$.

As S is a complex field, there will be two additional physical Higgs bosons in the NMSSM compared to the MSSM. For a CP-conserving theory (as is assumed here) we have three CP-even neutral states H_1, H_2, H_3 and two CP-odd neutral states A_1 and A_2 , where we take the states to be ordered in mass with H_1 and A_1 the lightest states.

The mass of the charged Higgs boson is at tree-level

$$m_{H^\pm}^2 = \frac{2\mu_{\text{eff}}}{\sin 2\beta}(A_\lambda + \kappa s) + m_W^2 - \lambda^2 v^2, \quad (2.3)$$

which can be compared with the MSSM expression $m_{H^\pm}^2 = m_A^2 + m_W^2$. It therefore simplifies our expressions to define an effective ‘‘doublet mass’’ in the NMSSM as

$$m_A^2 = \frac{2\mu_{\text{eff}}}{\sin 2\beta}(A_\lambda + \kappa s) = \frac{\lambda s}{s_\beta c_\beta}(A_\lambda + \kappa s) = \frac{\mu_{\text{eff}}}{s_\beta c_\beta}(A_\lambda + \frac{\kappa}{\lambda}\mu_{\text{eff}}), \quad (2.4)$$

where we defined $s_\beta = \sin \beta$ and $c_\beta = \cos \beta$. Thus, for fixed μ_{eff} , the squared doublet mass and the charged Higgs mass both depend linearly on A_λ and on κ/λ . The parameter A_λ may be everywhere swapped for m_A as a parameter of the Higgs sector. The mass relation (2.3) can then be written as

$$m_{H^\pm}^2 = m_A^2 + m_W^2 - \lambda^2 v^2. \quad (2.5)$$

This exhibits one important difference between the NMSSM and the MSSM: in the MSSM, the charged Higgs and the CP-odd Higgs are almost degenerate in mass as soon as they are heavier than $\sim 200 \text{ GeV}$. In the NMSSM there is no such strong correlation; partly because of the additional contribution $-\lambda^2 v^2$ which lowers $m_{H^\pm}^2$, but mainly because there is usually no physical state with mass m_A . The two CP-odd states in the NMSSM arise as mixtures of the CP-odd state of the MSSM, $A = \text{Im}(H_u c_\beta + H_d s_\beta)$, and of the imaginary part of the scalar S . The effective mass m_A thus only corresponds to a physical mass if the mixing between the two pseudoscalar bosons vanishes. This mixing is obtained from the mass matrix for A_1, A_2 ,

$$\mathcal{M}_P^2 = \begin{pmatrix} m_A^2 & \frac{v}{s}(m_A^2 s_\beta c_\beta - 3\lambda\kappa s^2) \\ \frac{v}{s}(m_A^2 s_\beta c_\beta - 3\lambda\kappa s^2) & \frac{v^2}{s^2} s_\beta c_\beta (m_A^2 s_\beta c_\beta + 3\lambda\kappa s^2) - 3\kappa A_\kappa s \end{pmatrix}. \quad (2.6)$$

In terms of the weak basis eigenstates $A_j^{\text{weak}} = (\text{Im } H_d, \text{Im } H_u, \text{Im } S)$, the physical CP-odd eigenstates $A_i^{\text{mass}} = (A_1, A_2)$ (ordered in increasing mass) are given by $A_i^{\text{mass}} = P_{ij} A_j^{\text{weak}}$ with the 2×3 mixing matrix P_{ij} , or explicitly

$$\begin{pmatrix} A_1 \\ A_2 \end{pmatrix} = \begin{pmatrix} P_{11} & P_{12} & P_{13} \\ P_{21} & P_{22} & P_{23} \end{pmatrix} \begin{pmatrix} \text{Im } H_d \\ \text{Im } H_u \\ \text{Im } S \end{pmatrix}.$$

It has been argued, for example by Dermisek and Gunion [9, 32–34], that A_1 may be much lighter than the other Higgs bosons, and can even be as light as a few GeV, and still be allowed by EWPT and collider constraints.

The masses of the CP-even Higgs states require a three-dimensional mixing matrix S_{ij} rotating the weak basis $H_j^{\text{weak}} = (\text{Re } H_d, \text{Re } H_u, \text{Re } S)$ to the physical one,

$$H_i^{\text{mass}} = S_{ij} H_j^{\text{weak}},$$

such that the physical mass eigenstates H_i^{mass} are ordered in increasing mass. The corresponding expressions for masses and mixings are omitted here; they may be found in e.g. [5]. It can be shown that the tree-level mass of the lightest Higgs boson H_1 is no longer limited by m_Z as in the MSSM, but instead by

$$m_{H_1}^2 \leq m_Z^2 \cos^2 2\beta + \lambda^2 v^2 \sin^2 2\beta. \quad (2.7)$$

To summarize, in the NMSSM (at tree-level), the lightest CP-even Higgs is allowed to be somewhat heavier, and the charged Higgs somewhat lighter, than in the MSSM, while the lightest CP-even Higgs may be much lighter than in the MSSM.

In the above discussion we have considered only the tree-level masses, but just as in the MSSM there can be considerable corrections to these masses at higher orders [35–42]. To take these into account to the best precision available [43], we use the code NMSSMTOOLS (version 2.3.5) [44, 45] for our numerical evaluation of the Higgs mass spectrum. We also use this code in the following to calculate the mixing, all coupling strengths, and the Higgs decay widths from the given input parameters.

Beyond leading order, the Higgs spectrum depends on all the parameters listed above, as well as on the soft SUSY-breaking parameters of other sectors; the most important corrections typically come from stop mixing. The standard way to cope with this situation in the MSSM is to consider a benchmark scenario (such as those defined in [46, 47]) to fix the higher order corrections from other SUSY sectors, and then vary independently the parameters in the Higgs sector. We shall use the same approach here, extending in a straightforward manner the MSSM benchmark scenario to the NMSSM. We therefore use μ_{eff} as an input, which together with the NMSSM coupling λ determines the value of the singlet vev s . Since we are mainly interested in comparing the NMSSM to the MSSM, rather than the MSSM to itself, we use the same benchmark (inspired by maximal mixing) throughout this work:

$$M_{\text{SUSY}} = 1 \text{ TeV}, \quad X_t^{\overline{\text{DR}}} \equiv A_t - \mu_{\text{eff}} \cot \beta = \sqrt{6} M_{\text{SUSY}}, \quad A_b = A_\tau = A_t \\ \mu_{\text{eff}} = 250 \text{ GeV}, \quad M_1 = 100 \text{ GeV}, \quad M_2 = 200 \text{ GeV}, \quad M_3 = 1 \text{ TeV}$$

For the remaining (free) input parameters of the NMSSM Higgs sector, we shall take A_λ , $\tan \beta$ —which are equivalent to the two parameters m_{H^\pm} , $\tan \beta$ in the MSSM through Eqs. (2.4), (2.5)—and in addition λ , κ , and A_κ , which are specific to NMSSM. For any choice of NMSSM parameters, the corresponding MSSM limit can be obtained by taking $\lambda \rightarrow 0$, $\kappa \rightarrow 0$, while keeping the ratio κ/λ and all dimensionful parameters fixed.

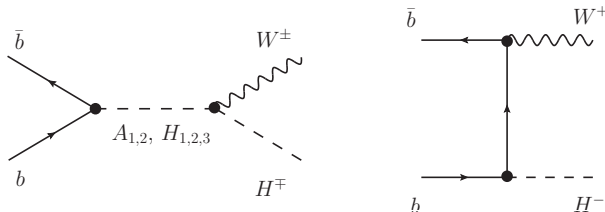


FIG. 1. Leading-order diagrams for the quark-initiated hard subprocess $b\bar{b} \rightarrow H^\pm W^\mp$.

III. ASSOCIATED $H^\pm W^\mp$ PRODUCTION

Associated $H^\pm W^\mp$ production has two contributing subprocesses at leading order, quark-antiquark ($q\bar{q}$) and gluon-gluon (gg) scattering. The leading order contributions correspond to the tree-level for $q\bar{q}$, and one loop for gg fusion. Representative diagrams for these subprocesses are depicted in Figs. 1 and 2, respectively. Working in a five-flavor scheme (5FS) with an effective parton distribution for the b quark, the $q\bar{q}$ process is completely dominated by the $b\bar{b}$ contribution. Although the cross section for gg fusion is formally suppressed by two powers of the QCD coupling α_s relative to $b\bar{b}$ annihilation, it may yield a comparable contribution at LHC energies due to the large gluon density at small x and needs to be taken into account. In the 5FS, there are additional contributions at higher orders of α_s where one gluon splits into a $b\bar{b}$ pair, giving $bg \rightarrow H^\pm W^\mp b$. These contributions should in principle be matched to the $b\bar{b} \rightarrow H^\pm W^\mp$ process, which would yield an effective QCD correction factor slightly less than one [14]. For simplicity we ignore this factor throughout this work. If the charged Higgs boson is light enough ($m_{H^\pm} < m_t$), there is an additional contribution to $H^\pm W^\mp$ production through top quark decays $t \rightarrow bH^\pm$. When \hat{s} is close to the $t\bar{t}$ threshold $\hat{s} \sim 4m_t^2$, on-shell top quarks can therefore give an additional production channel $gg \rightarrow t\bar{t} \rightarrow H^\pm W^\mp b\bar{b}$, which is enhanced by top resonances. However, in this work we study the case when the H^\pm boson is heavy enough to be above the threshold for production in top decays, and this extra production channel is not relevant.

The next-to-leading order (NLO) corrections to the $H^\pm W^\mp$ cross section in the MSSM are known [19–24], but for the present study the leading order contributions suffice since we are mainly interested in comparing the NMSSM to the MSSM. We will, however, account for the most important higher order contributions from running quark masses, loop corrections to Higgs masses and mixings, and including (mass-dependent) widths of Higgs bosons appearing in s -channel propagators. The treatment of these effects is described in further detail below.

Consider first the $b\bar{b} \rightarrow H^\pm W^\mp$ contribution, which to the leading order is given by the tree-level diagrams in Fig. 1. At the parton-level, this contribution typically dominates over the gluonic one considered below. The corresponding parton-level cross section has the same form as in the MSSM case [14],

$$\begin{aligned}
\frac{d\hat{\sigma}}{d\hat{t}}(b\bar{b} \rightarrow H^+W^-) &= \frac{G_F^2}{24\pi\hat{s}} \left\{ \frac{m_b^2}{2} \lambda(\hat{s}, m_W^2, m_{H^\pm}^2) \left(|\mathcal{S}_b(\hat{s})|^2 + |\mathcal{P}_b(\hat{s})|^2 \right) \right. \\
&\quad + \frac{m_b^2 \tan \beta}{\hat{t} - m_t^2} \left(m_W^2 m_{H^\pm}^2 - \hat{s} p_\perp^2 - \hat{t}^2 \right) \text{Re} \left[\mathcal{S}_b(\hat{s}) - \mathcal{P}_b(\hat{s}) \right] \\
&\quad \left. + \frac{1}{(\hat{t} - m_t^2)^2} \left[m_t^4 \cot^2 \beta \left(2m_W^2 + p_\perp^2 \right) + m_b^2 \tan^2 \beta \left(2m_W^2 p_\perp^2 + \hat{t}^2 \right) \right] \right\}, \tag{3.1}
\end{aligned}$$

where G_F is the Fermi constant, \hat{s} , \hat{t} , \hat{u} are the usual Mandelstam variables, p_\perp is the transverse momentum of the W boson in the $b\bar{b}$ c.m. frame, and $\lambda(x, y, z) = x^2 + y^2 + z^2 - 2(xy + yz + zx)$ is the Källén function. The first line in Eq. (3.1) represents the s -channel resonance contribution, the last line corresponds to the non-resonant top quark exchange in the t -channel, and the second line contains the interference term.

The functions \mathcal{S}_q and \mathcal{P}_q contain the propagators and relative couplings for the neutral Higgs bosons to quark flavor q . In Eq. (3.1) only the b quark contribution is needed, but for the gg contribution discussed below we need also the corresponding expressions for the top quark. These functions are defined as

$$\begin{aligned}\mathcal{S}_t(\hat{s}) &= \frac{1}{\sin\beta} \sum_{i=1,2,3} \frac{S_{i2} (S_{i2} \cos\beta - S_{i1} \sin\beta)}{\hat{s} - m_{H_i}^2 + im_{H_i}\Gamma_{H_i}}, \\ \mathcal{S}_b(\hat{s}) &= \frac{1}{\cos\beta} \sum_{i=1,2,3} \frac{S_{i1} (S_{i2} \cos\beta - S_{i1} \sin\beta)}{\hat{s} - m_{H_i}^2 + im_{H_i}\Gamma_{H_i}}, \\ \mathcal{P}_t(\hat{s}) &= \frac{1}{\sin\beta} \sum_{i=1,2} \frac{P_{i2} (P_{i2} \cos\beta - P_{i1} \sin\beta)}{\hat{s} - m_{A_i}^2 + im_{A_i}\Gamma_{A_i}}, \\ \mathcal{P}_b(\hat{s}) &= -\frac{1}{\cos\beta} \sum_{i=1,2} \frac{P_{i1} (P_{i2} \cos\beta - P_{i1} \sin\beta)}{\hat{s} - m_{A_i}^2 + im_{A_i}\Gamma_{A_i}},\end{aligned}\tag{3.2}$$

where Γ_{H_i} and Γ_{A_i} are the total (mass-dependent) decay widths of the H_i and A_i bosons, respectively. We have obtained the expressions given in Eq. (3.2) by modifying the \mathcal{S} , \mathcal{P} functions given in [14] with the appropriate Yukawa couplings for the NMSSM case. We neglect the Yukawa couplings of the first- and second-generation quarks, as their contributions to the amplitude are negligibly small. If the masses of two (or more) neutral Higgs bosons with the same CP properties become degenerate, then the approximation used in Eq. (3.2) breaks down, and one has to take into account Higgs mixing effects (see e.g. Refs. [48, 49]). For the NMSSM scenarios we shall consider below, the masses will however always be such that Eq. (3.2) remain valid.

Let us now turn to the gg contribution. In analogy to the MSSM case [14–17], the resonant amplitude of the $gg \rightarrow H_{1,2,3}, A_{1,2} \rightarrow H^\pm W^\mp$ subprocess from quark loops is given by the sum of all triangle diagrams of the type shown as the first diagram (upper left) in Fig. 2. This contribution can be written as

$$\begin{aligned}V_{\lambda_W}^\Delta &= \frac{\sqrt{2}}{\pi} \alpha_s(\mu_R) G_F m_W \epsilon_\gamma^*(p_W) (q_1 + q_2)^\gamma \\ &\times \epsilon_\mu^c(q_1) \epsilon_\nu^c(q_2) \left[\left(q_2^\mu q_1^\nu - \frac{\hat{s}}{2} g^{\mu\nu} \right) \Sigma(\hat{s}) + i \epsilon^{\mu\nu\rho\sigma} q_{1\rho} q_{2\sigma} \Pi(\hat{s}) \right],\end{aligned}\tag{3.3}$$

where $\alpha_s(\mu_R)$ is the strong coupling evaluated at the renormalization scale μ_R , ϵ_γ^* is the polarization vector of the W boson with momentum p_W and helicity λ_W , and $\epsilon_{\mu,\nu}^c$ are the polarization vectors of the gluons with momenta $q_{1,2}$. These are summed over the color index c . The functions Σ and Π come from the loop integration and correspond to neutral CP-even $H_{1,2,3}$ exchanges (Σ) and neutral CP-odd $A_{1,2}$ exchanges (Π) in the s -channel. They

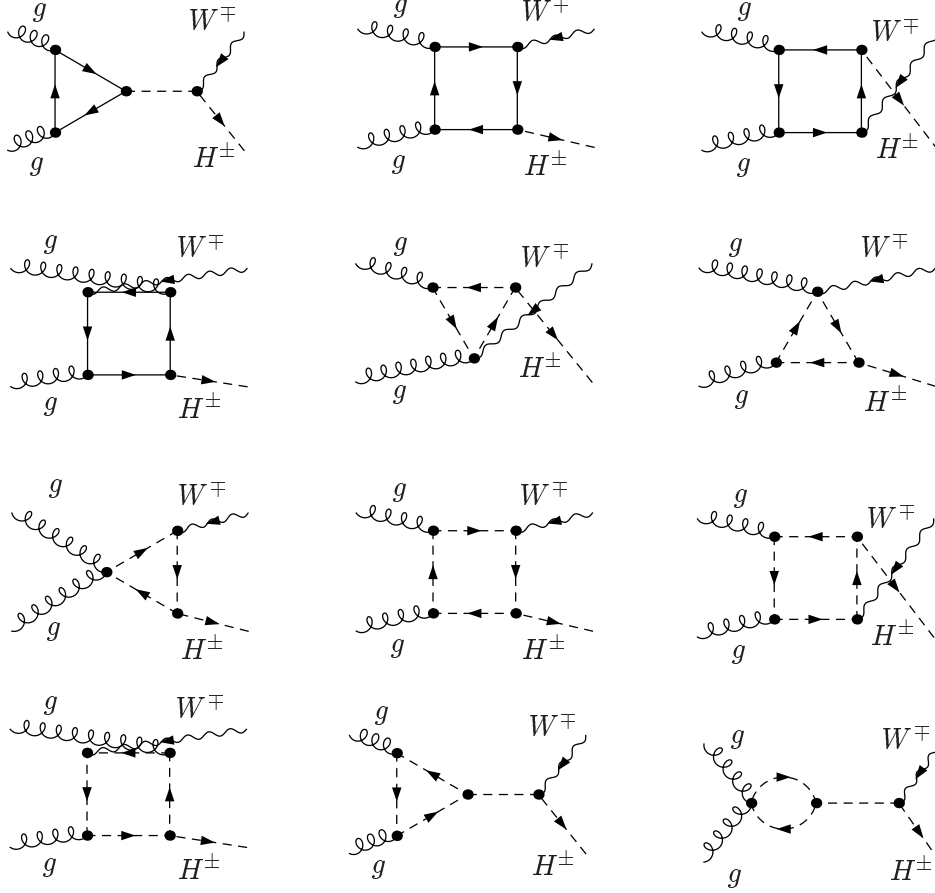


FIG. 2. Example leading-order diagrams contributing to the gluon-initiated hard subprocess $gg \rightarrow H^\pm W^\mp$. Dashed lines with arrows represent squarks, while internal dashed lines without arrows represent neutral Higgs bosons ($H_{1,2,3}, A_{1,2}$). Only the diagrams with internal s -channel Higgs propagators will give rise to the resonant enhancement we are discussing in this paper.

are given by

$$\Sigma(\hat{s}) = \sum_q \mathcal{S}_q(\hat{s}) S\left(\frac{\hat{s} + i\epsilon}{4m_q^2}\right), \quad (3.4)$$

$$\Pi(\hat{s}) = \sum_q \mathcal{P}_q(\hat{s}) P\left(\frac{\hat{s} + i\epsilon}{4m_q^2}\right), \quad (3.5)$$

where the sums run over all quark flavors q in the triangle loops, and the functions

$$S(r) = \frac{1}{r} \left[1 - \left(1 - \frac{1}{r} \right) \operatorname{arcsinh}^2 \sqrt{-r} \right], \quad (3.6)$$

$$P(r) = -\frac{1}{r} \operatorname{arcsinh}^2 \sqrt{-r}, \quad (3.7)$$

must be continued analytically for three regions in r , such that for $r \leq 0$, $0 < r \leq 1$, or $r > 1$, $\operatorname{arcsinh}\sqrt{-r}$ must be represented by $\operatorname{arcsinh}\sqrt{-r}$, $-\mathrm{i}\arcsin\sqrt{r}$, or $\operatorname{arccosh}\sqrt{r} - \mathrm{i}\pi/2$, respectively. The contribution to the parton-level cross section is then given by

$$\frac{d\hat{\sigma}^\Delta}{d\hat{t}}(gg \rightarrow H^+W^-) = \frac{\alpha_s^2(\mu_R)G_F^2}{2048\pi^3}\lambda(\hat{s}, m_W^2, m_{H^\pm}^2)\left(|\Sigma(\hat{s})|^2 + |\Pi(\hat{s})|^2\right). \quad (3.8)$$

Due to Bose symmetry, the $gg \rightarrow H^\pm W^\mp$ cross section is symmetric with respect to $\hat{t} \leftrightarrow \hat{u}$ interchange. Additionally, since we only consider the CP-invariant case, the cross sections for the $gg \rightarrow H^+W^-$ and $gg \rightarrow H^-W^+$ channels coincide.

In our numerical calculations we take all possible quark and squark loop contributions into account from both triangle and box diagrams. For simplicity, we show here only the formulas for quark triangles, and do not list the complicated expressions for either the boxes or the diagrams with squark loops, schematically shown in Fig. 2. The full result also includes interference between these different contributions. We have checked our numerical results in the MSSM limit (which will be described below) against previous results from the literature [14, 24].

Formally, the leading order contributions (as given by Eqs. (3.2)–(3.8) above) contain tree-level masses and couplings. As advocated previously (see [24] and references therein), higher order QCD and electroweak corrections can significantly affect MSSM observables. In particular the bottom Yukawa coupling is subject to large quantum corrections in the MSSM—as well as in the NMSSM—and these need to be taken into account properly. For this purpose, we follow the general recipe given in [24]. To take into account the large (SM) QCD corrections to the leading-order result, we use the QCD running b quark mass $m_b = m_b^{\overline{\text{DR}}}(\mu_R)$. At two-loop order it is given by [50]

$$m_b^{\overline{\text{DR}}}(\mu_R) = m_b^{\overline{\text{MS}}}(\mu_R)\left[1 - \frac{\alpha_s}{3\pi} - \frac{\alpha_s^2}{144\pi^2}(73 - 3n)\right], \quad (3.9)$$

where n is the number of active quark flavors and $m_b^{\overline{\text{MS}}}(\mu_R)$ is the standard $\overline{\text{MS}}$ running mass (we use $m_b^{\overline{\text{MS}}}(m_b) = 4.2$ GeV as input). Then, including the $\tan\beta$ -enhanced supersymmetric QCD (SQCD) and electroweak (SEW) corrections [51] by a straightforward generalization of the MSSM results [52], we obtain the following effective bottom-Higgs couplings:

$$\lambda_{b\bar{b}H_i}^{\text{eff}} = -\mathrm{i}\frac{m_b^{\overline{\text{DR}}}}{\sqrt{2}v\cos\beta}\frac{S_{i1}}{1 + \Delta_b}\left(1 + \Delta_b\frac{S_{i2}}{S_{i1}\tan\beta}\right), \quad i = 1, 2, 3 \quad (3.10)$$

$$\lambda_{b\bar{b}A_k}^{\text{eff}} = \frac{m_b^{\overline{\text{DR}}}}{\sqrt{2}v\cos\beta}\frac{P_{k1}}{1 + \Delta_b}\left(1 + \Delta_b\frac{P_{i2}}{P_{i1}\tan\beta}\right), \quad k = 1, 2 \quad (3.11)$$

In a similar manner we also include the relevant corrections to the H^+tb vertex [53]. These so-called Δ_b corrections consist of two dominating parts, $\Delta_b = \Delta_b^{\text{SQCD}} + \Delta_b^{\text{SEW}}$, absorbing the leading SQCD and SEW corrections. In our case, the latter is dominated by the Higgsino-stop contribution $\Delta_b^{\text{SEW}} \simeq \Delta_b^{\tilde{H}t}$. In complete analogy to the MSSM case we therefore have $\Delta_b \simeq \Delta_b^{\text{SQCD}} + \Delta_b^{\tilde{H}t}$, where

$$\Delta_b^{\text{SQCD}} = \frac{2\alpha_s(Q)}{3\pi}m_{\tilde{g}}\mu_{\text{eff}}\tan\beta I(m_{\tilde{b}_1}^2, m_{\tilde{b}_2}^2, m_{\tilde{g}}^2), \quad Q = (m_{\tilde{b}_1} + m_{\tilde{b}_2} + m_{\tilde{g}})/3,$$

$$\Delta_b^{\tilde{H}t} = \frac{m_t^2}{16\pi^2v^2\sin^2\beta}A_t\mu_{\text{eff}}\tan\beta I(m_{\tilde{t}_1}^2, m_{\tilde{t}_2}^2, |\mu_{\text{eff}}|^2),$$

and finally

$$I(a, b, c) = -\frac{1}{(a-b)(b-c)(c-a)} \left(ab \ln \frac{a}{b} + bc \ln \frac{b}{c} + ca \ln \frac{c}{a} \right).$$

Here $m_{\tilde{g}}$ denotes the gluino mass, and $m_{\tilde{b}_i}$, $m_{\tilde{t}_i}$ ($i = 1, 2$) the sbottom and stop masses. From these expressions it is clear that the Δ_b corrections could become large for either large values of μ_{eff} and/or large $\tan \beta$.

We shall refer below to the calculation at leading order, including the improvements discussed here (higher order corrections to Higgs masses and mixing, the Higgs widths in the s -channel Higgs propagators, the running m_b , and the SUSY corrections to the bottom Yukawa couplings), as the *improved Born approximation*.

To calculate the cross sections and perform the numerical computations, we have modified and extended the MSSM model file [54] of FEYNARTS [55] to contain the relevant NMSSM couplings and the necessary steps to use the improved Born approximation as discussed above. The parton-level amplitudes have been computed with FORMCALC [56] and integrated numerically. For the evaluation of the scalar master tree- and four-point integrals in the gluon contribution we have used the LOOPTOOLS library [56]. The Higgs mass spectra, mixing, couplings and decay widths have been calculated using NMSSMTOOLS [44, 45].

IV. RESULTS

A. NMSSM parameter dependence and benchmark scenarios

As a first step, we investigate the impact on the parton-level cross sections $\hat{\sigma}_{b\bar{b} \rightarrow H^\pm W^\mp}$ and $\hat{\sigma}_{g\bar{g} \rightarrow H^\pm W^\mp}$ of varying the NMSSM parameters. This information will be useful for defining the benchmark scenarios we are going to study in more detail below. We start from a generic NMSSM scenario with parameter values chosen as follows (this is what we will below refer to as Scenario A):

$$\begin{aligned} \lambda &= 0.25, & \kappa &= 0.25, & A_\lambda &= -235 \text{ GeV}, \\ A_\kappa &= -150 \text{ GeV}, & \tan \beta &= 10, \end{aligned} \tag{4.1}$$

and perform variations around these values. For each parameter point the partonic cross sections are evaluated as a function of $\sqrt{\hat{s}}$, using the improved Born approximation as described in Section III.

To be able to study genuine NMSSM effects on the $H^\pm W^\mp$ process, we first want to compare our results to those obtained in the MSSM limit. We therefore look at the behavior of the partonic cross sections during the gradual transition from the NMSSM point defined by the parameter set given by Eq. (4.1) to the corresponding MSSM limit.¹ The results are shown in Fig. 3. A striking difference between the NMSSM and the MSSM is the presence of resonant enhancement of the partonic cross sections in the NMSSM. These resonances can be attributed to the heavy neutral Higgs poles $\hat{s} = m_{H_3}^2$ and $\hat{s} = m_{A_2}^2$, which for the default parameters have masses $m_{H_3} = 462.6 \text{ GeV}$ and $m_{A_2} = 349.3 \text{ GeV}$ (see Table I below). Since in the MSSM it is generally true that $m_{H,A} < m_{H^\pm}$, these resonant contributions vanish in the MSSM limit. They are therefore an inherent feature of the NMSSM. As we will

¹ We remind the reader that the MSSM limit is defined by taking $\lambda, \kappa \rightarrow 0$, while keeping the ratio κ/λ and all other parameters fixed to their respective values.

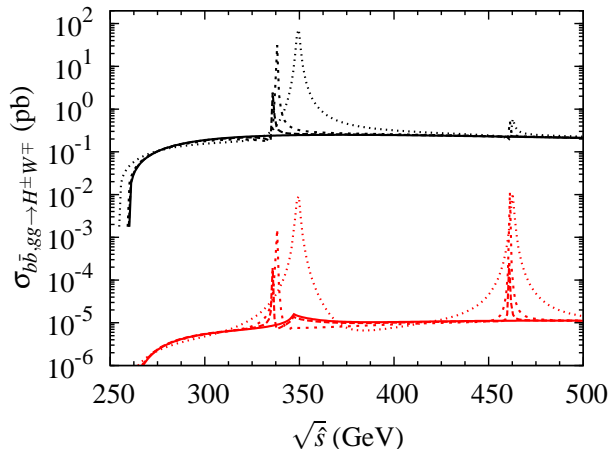


FIG. 3. Parton-level cross sections for $H^\pm W^\mp$ production by $b\bar{b}$ (black) and gg (red) initial states for $\lambda = \kappa = 0.25$ (dotted), 0.1 (short-dashed), 0.05 (long-dashed), and in the MSSM limit $\lambda = \kappa = 10^{-10}$ (solid). The remaining NMSSM parameters are fixed according to the description given in the text.

show below, the resonant contributions are sensitive to the NMSSM parameters, and can give important contributions to the rate for $pp \rightarrow H^\pm W^\mp$ production. They are therefore interesting to study as a means of discriminating between the two models.

Having established the presence of resonances as a potentially important difference for $H^\pm W^\mp$ production between the MSSM and NMSSM, we now proceed to study how the characteristics of these resonances are affected by variation of the NMSSM parameters. The results are shown in Fig. 4. Starting from the upper left plot, we first consider different values of A_λ . This has an immediate effect on the threshold through the linear dependence of $m_{H^\pm}^2$ on A_λ (see Eq. (2.3)). It can also be seen that a change in A_λ affects the presence of a resonance peak in the cross section. Qualitatively this can be understood from the fact that a charged Higgs boson with lower m_{H^\pm} can be produced from a (nearly) singlet scalar (pseudoscalar) of fixed mass, while this possibility disappears for a particular mass as m_{H^\pm} is increased. Further details on this point will be given below. Moving to the next plot, we see that a variation of A_κ affects the cross sections in quite a different manner; it affects the relative positions and sizes of the resonance peaks. Effectively, when going from low $|A_\kappa|$ to higher values the two peaks, which at first are well separated, first meet and then get separated again, having changed positions. Since it also affects the relative size of the peaks, this signals that the mixture of the neutral Higgs resonances changes with modified A_κ . The two plots in the second row show the variation with λ and κ , respectively. In addition to the similar shift in threshold as demonstrated for the A_λ case, we also see that these cross sections appear to depend on these parameters in the same combination as appears in m_{H^\pm} for fixed μ_{eff} , that is through the ratio κ/λ . On the last row of Fig. 4 we show the variation of the cross sections with μ_{eff} . This gives a very similar effect as choosing different values for A_λ , which motivates us to consider a fixed value $\mu_{\text{eff}} = 250$ GeV in the following and instead use variation of A_λ to control the value of m_{H^\pm} . The final plot shows the effect of a $\tan\beta$ variation. Also this variable enters the determination of m_{H^\pm} (and thereby shifts the threshold), although in a more indirect way than μ_{eff} or A_λ . As can be seen from the figure, changing $\tan\beta$ also has a drastic effect on the absolute normalization of the cross sections and the width of the resonances. This comes mainly from the coupling of the charged Higgs boson to fermions of the third generation. For equivalent kinematic configurations, we can

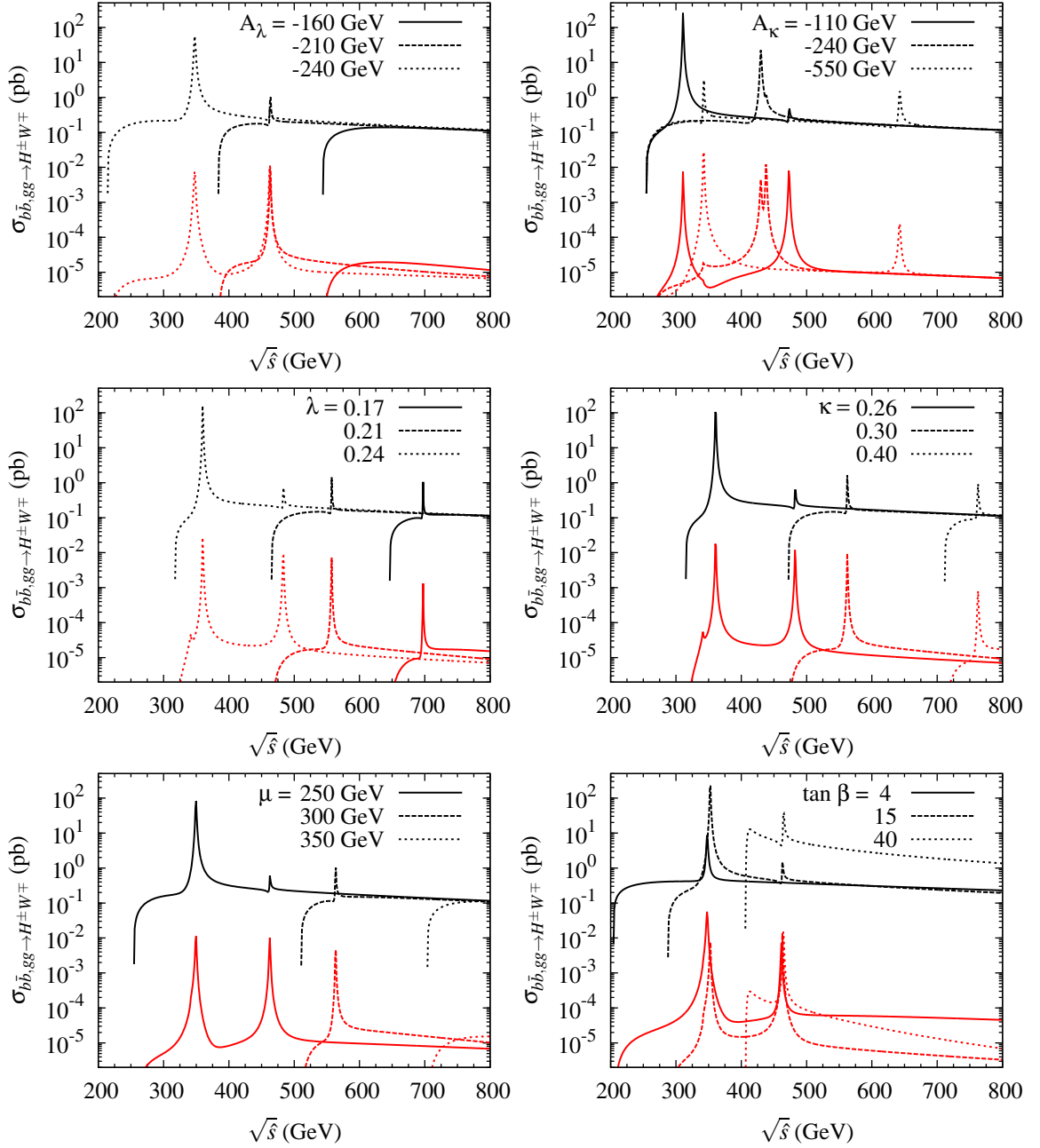


FIG. 4. Parton-level cross sections for $H^\pm W^\mp$ production by $b\bar{b}$ (black) and gg (red) initial states versus $\sqrt{\hat{s}}$ for different values of the NMSSM parameters, as indicated in the plots. The remaining NMSSM parameters are fixed according to the description in the text.

therefore expect enhancements of the cross sections either for small or large values of $\tan \beta$.

Based on these parameter variations we define five benchmark scenarios for further study (called scenarios A–E). The scenarios are selected to capture the different features of the partonic cross sections discussed above, and the values for the input parameters in the five benchmarks are shown in Table I. This table also gives the resulting Higgs mass spectrum, and the $S_{3,3}$, $P_{2,3}$ elements of the Higgs mixing matrices which give the singlet fractions of the heavy Higgs bosons H_3 and A_2 . They will be relevant for the discussion of the resonant

Parameter	Scenario				
	A	B	C	D	E
A_λ (GeV)	-235	-235	-235	-185	-243
A_κ (GeV)	-150	-250	-400	-150	-150
λ	0.25	0.25	0.25	0.5	0.25
κ	0.25	0.25	0.25	0.5	0.25
$\tan\beta$	10	10	10	2.2	40
Higgs mass spectrum (GeV)					
m_{H^\pm}	174.3	174.3	174.3	195.3	171.7
m_{H_1}	118.4	117.4	115.0	114.6	120.3
m_{H_2}	173.5	174.1	174.3	203.6	246.0
m_{H_3}	462.6	435.3	391.1	459.6	463.3
m_{A_1}	139.0	156.4	165.4	92.0	213.2
m_{A_2}	349.3	438.2	549.2	383.4	355.7
Singlet elements of H_3, A_2					
$S_{3,3}$	0.993	0.991	0.986	0.988	0.992
$P_{2,3}$	0.945	0.981	0.993	0.875	0.897

TABLE I. Selected NMSSM benchmark scenarios, the corresponding Higgs mass spectrum, and singlet elements $S_{3,3}$, $P_{2,3}$ of the Higgs mixing matrices for the neutral heavy Higgs bosons.

contributions below.

Table I shows some features which are common to all the scenarios. As a general strategy we choose the parameters to obtain a rather low m_{H^\pm} in all scenarios (but still keeping $m_{H^\pm} > m_t$). For compatibility with LEP constraints [57], we make sure that the lightest CP-even Higgs mass $m_{H_1} > 114.4$ GeV.² The scenarios are also compatible with the limits from direct Higgs searches at the Tevatron and the LHC implemented in HIGGS-BOUNDS v.2.1.0 [58]. Going into the specifics of the individual scenarios, the only difference between the definitions of scenarios A, B, and C is the value for A_κ . This variation leads to three different hierarchies for m_{H_3} and m_{A_2} , as can be read off from the table. Scenarios D and E are both mostly similar to Scenario A in terms of the heavy Higgs mass structure. Here we instead consider two “extreme” cases of low (D) and high (E) values for $\tan\beta$.

B. Parton-level cross sections

We now proceed to study associated $H^\pm W^\mp$ production in the NMSSM, making use of the benchmark scenarios defined in the previous section. The parton-level cross sections are evaluated as described in Section III, and the results for $\hat{\sigma}_{b\bar{b} \rightarrow H^\pm W^\mp}$ are shown in Fig. 5.

In this figure the solid lines give the NMSSM cross sections, while the dashed lines are the corresponding cross sections in the MSSM limit. As already discussed above, the most

² Applying this limit to the NMSSM in general is a very conservative approach, since it strictly speaking only applies to a Higgs with SM-like couplings. Specific NMSSM scenarios admit $m_{H_1} \ll 114.4$ GeV without being in conflict with experimental data. However, in this work the selected scenarios correspond to the case where H_1 is SM-like, and therefore the SM limit applies.

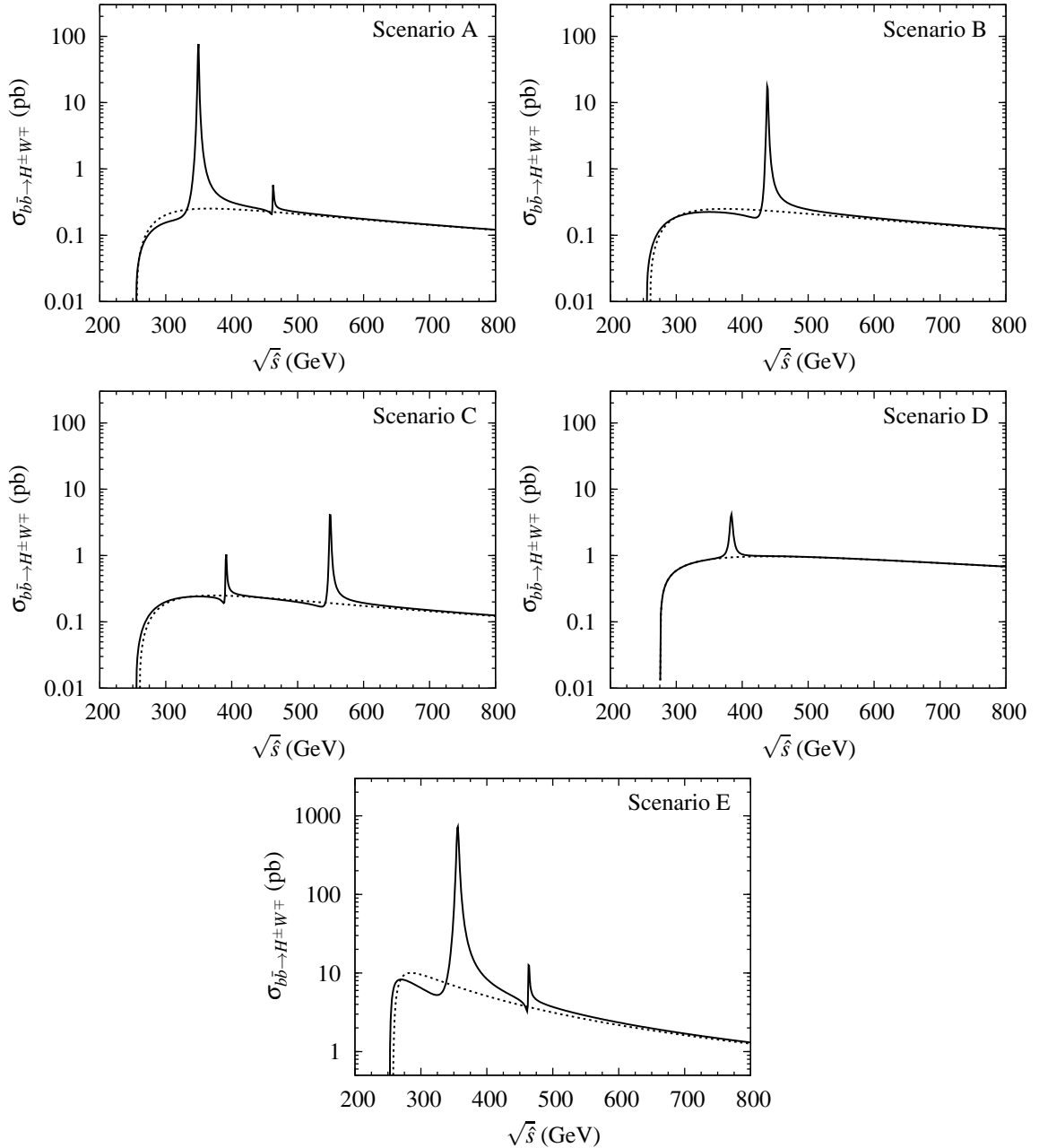


FIG. 5. Partonic cross sections $\hat{\sigma}_{b\bar{b} \rightarrow H^\pm W^\mp}$ for NMSSM benchmark scenarios A–E (solid lines), and the corresponding results in the MSSM limit (dashed).

striking difference is the presence of resonances in the NMSSM case. In all the five benchmarks the resonances are manifest as either one or two peaks of varying size. Comparing the plots for scenarios A–C, we observe a shift of the large peak from low energies (for Scenario A) to high energies (Scenario C). There is also a corresponding down-shift of the smaller peak to low energies. For Scenario B the two peaks nearly coincide. The positions of these poles are determined by m_{H_3} and m_{A_2} , and we note that the largest peak corresponds to the A_2 resonance. This means that even if the singlet component of A_2 is larger than that of H_3 ($|P_{2,3}| > |S_{3,3}|$), the A_2 couples more strongly to the $b\bar{b}$ initial state. For Scenario D we only observe one (small) resonance peak. This is due to the low value of $\tan\beta$, corresponding to

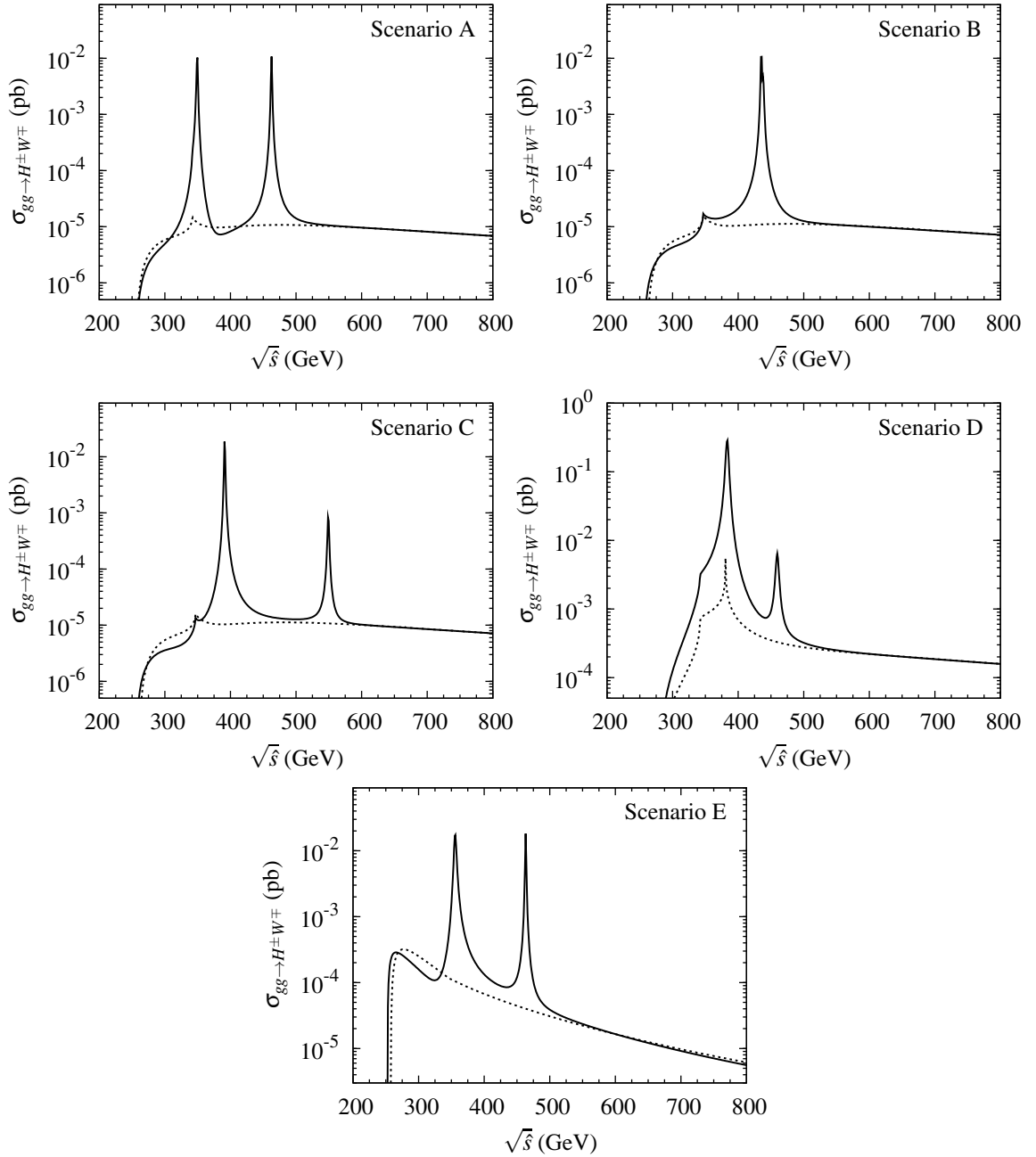


FIG. 6. Partonic cross sections $\hat{\sigma}_{gg \rightarrow H^\pm W^\mp}$ for NMSSM benchmark scenarios A–E (solid lines), and the corresponding results in the MSSM limit (dashed).

a reduced $A_2 b \bar{b}$ coupling. On the other hand, we also observe a larger overall cross section in the continuum (visible also in the MSSM limit), since the non-resonant contribution mediated by t -channel top exchange increases as $\tan \beta \ll 7$. For Scenario E (which has a high value of $\tan \beta$) something similar is observed for the continuum, but with an even larger enhancement of the cross section at low energies and a more rapid drop as $\sqrt{\hat{s}} \rightarrow \infty$. In this case we also observe two pronounced resonances (as in scenarios A and C), but the fairly large couplings in Scenario E lead to larger differences between the NMSSM results and the MSSM limit also for energies away from the actual poles.

Turning now to $\hat{\sigma}_{gg \rightarrow H^\pm W^\mp}$, the contribution from gluon fusion is expected to be richer than that initiated by b -quarks, since it involves additional non-resonant box diagrams. The interference with these can strongly affect the resulting cross section (for a study of these interference effects in the MSSM, see [14]). The cross section is again evaluated as outlined in Section III and the results are shown in Fig. 6. One look at this figure reveals that the gluon-initiated process has a much lower cross section compared to the $b\bar{b}$ initial state, about 3–4 orders of magnitude. We can however expect this difference to be (at least partly) compensated in the hadronic cross section by the larger gluon content of the proton at intermediate and small x (see below). Compared to the $b\bar{b}$ process, we do observe a general broadening of the resonances, and larger differences between the NMSSM and the MSSM limit—the latter in particular for energy ranges between near-lying resonances, where interference can lead to either an enhanced or suppressed cross section prediction in the NMSSM compared to the MSSM. Most of the gg distributions show a feature at the top pair threshold $\sqrt{\hat{s}} = 2m_t$ (sometimes masked by an NMSSM resonance). Since this kinematic effect is present also in the MSSM it is not interesting for the comparison of the results between the two models.

Looking specifically at the results for scenarios A–C in Fig. 6, they display the same resonance structure as the $b\bar{b}$ case. This tells us that both the H_3 and A_2 resonances play a role also here. However the peaks are more similar in size (for Scenario A), and in the case of Scenario C we see that the low energy peak is dominating the cross section. Since this corresponds to the H_3 contribution, we conclude that the resonant process here is instead dominated by the $H_3 t\bar{t}$ coupling which enters the top loop contribution. The importance of the coupling to the top for lower $\tan\beta$ becomes evident for Scenario D. This scenario has a greatly enhanced cross section, both compared to scenarios A–C, and with very pronounced resonance enhancements compared to the MSSM limit. Also Scenario E benefits from the same large continuum cross section as observed for the $b\bar{b}$ contribution, but with the additionally boosted resonance contribution of H_3 observed generally for the gg process.

C. Hadron-level cross sections

The total hadronic cross section $\sigma_{pp \rightarrow H^\pm W^\mp}$ is obtained from the partonic cross sections $\hat{\sigma}_{ij}$ (with $ij = b\bar{b}, gg$) by integration over the parton distribution functions (PDFs). This can alternatively be expressed in terms of parton luminosities, which allows studying the impact of the PDFs on the cross section. The parton luminosities L_{ij} for partons i, j are defined as

$$\tau \frac{dL_{ij}}{d\tau} = \int dx_1 dx_2 x_1 x_2 \delta(\tau - x_1 x_2) \left\{ f_i(x_1, \mu_F^2) f_j(x_2, \mu_F^2) + i \leftrightarrow j \right\}, \quad (4.2)$$

where $\tau = x_1 x_2$ and $f_i(x, \mu_F^2)$ is the PDF for parton i evaluated at the factorization scale μ_F . Note that, since we are interested in $b\bar{b}$ and gg scattering, we will always have $f_i(x) = f_j(x)$. The significance of τ is that the center-of-mass energy of the partonic system is given by $\sqrt{\hat{s}} = \sqrt{\tau s}$, where $\sqrt{s} = E_{\text{CM}}$ is the collider energy. Using the parton luminosities, the total cross section can be expressed as

$$\sigma_{pp \rightarrow H^\pm W^\mp}(s) = \int_0^1 \frac{d\tau}{\tau} \left[\frac{1}{s} \frac{dL_{ij}}{d\tau} \right] [\hat{s} \hat{\sigma}_{ij}(\hat{s})]. \quad (4.3)$$

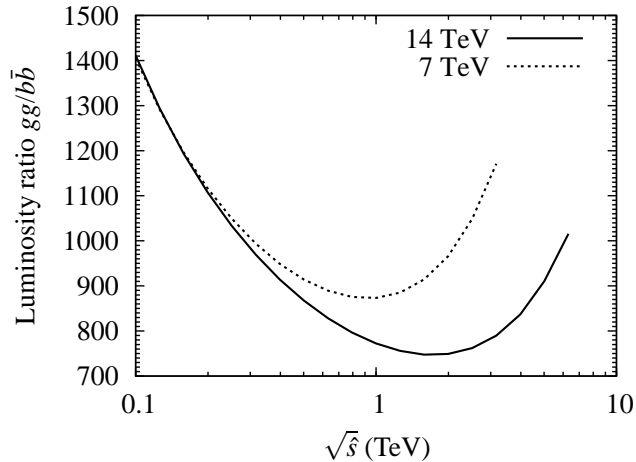


FIG. 7. Ratio of parton luminosities $(dL_{gg}/d\hat{s})/(dL_{b\bar{b}}/d\hat{s})$ at 14 TeV (solid) and 7 TeV (dotted).

Note that the factor involving the parton luminosity has the dimensions of a cross section; it can be used to estimate the size of the hadronic cross section when the partonic cross section is known. Even though the gg cross sections are much smaller than the $b\bar{b}$ cross sections at parton-level, at hadron-level the much larger gluon PDFs make the gg contribution competitive with the $b\bar{b}$ contribution. In Fig. 7 we show the ratio of the gg and $b\bar{b}$ luminosities at 7 TeV and at 14 TeV, calculated with MSTW PDFs [59]. We see from this figure that the $gg/b\bar{b}$ luminosity ratio is typically a factor 1000 at 7 TeV, and slightly smaller for 14 TeV.

For the calculation of the hadronic cross sections, we modify the benchmark scenarios listed in Table I to allow for variation of m_{H^\pm} . This is achieved by varying the value of A_λ , keeping the other parameters fixed to the values given in the table. Besides changing m_{H^\pm} , this affects the doublet-dominated neutral Higgs bosons (which never appear resonantly), while the masses of the singlet-dominated Higgses (H_3 and A_2 for low m_{H^\pm}) are largely insensitive to A_λ variations. This means in particular that the resonance structure discussed

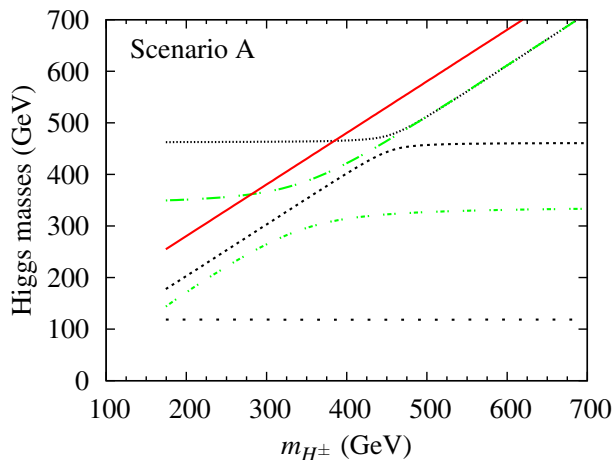


FIG. 8. Dependence of the neutral Higgs masses on m_{H^\pm} in Scenario A with varying charged Higgs boson mass. The different curves correspond to (in black): m_{H_1} (sparse dots), m_{H_2} (dotted), m_{H_3} (dense dots), and in green m_{A_1} (dot-dashed, short), and m_{A_2} (dot-dashed, long). The solid red line shows the threshold for associated $H^\pm W^\mp$ production.

above will remain unaltered over certain ranges for m_{H^\pm} (when the doublet mass is well below the singlet mass scale). This important point is demonstrated in Fig. 8, which shows the dependence of the five neutral Higgs masses in Scenario A on m_{H^\pm} (when varying A_λ). A qualitatively similar picture is obtained in the other scenarios we study.

For the numerical evaluation of the cross sections we consider pp collisions at the LHC at the two center of mass energies $\sqrt{s} = 7$ TeV and $\sqrt{s} = 14$ TeV. We use CTEQ6.6

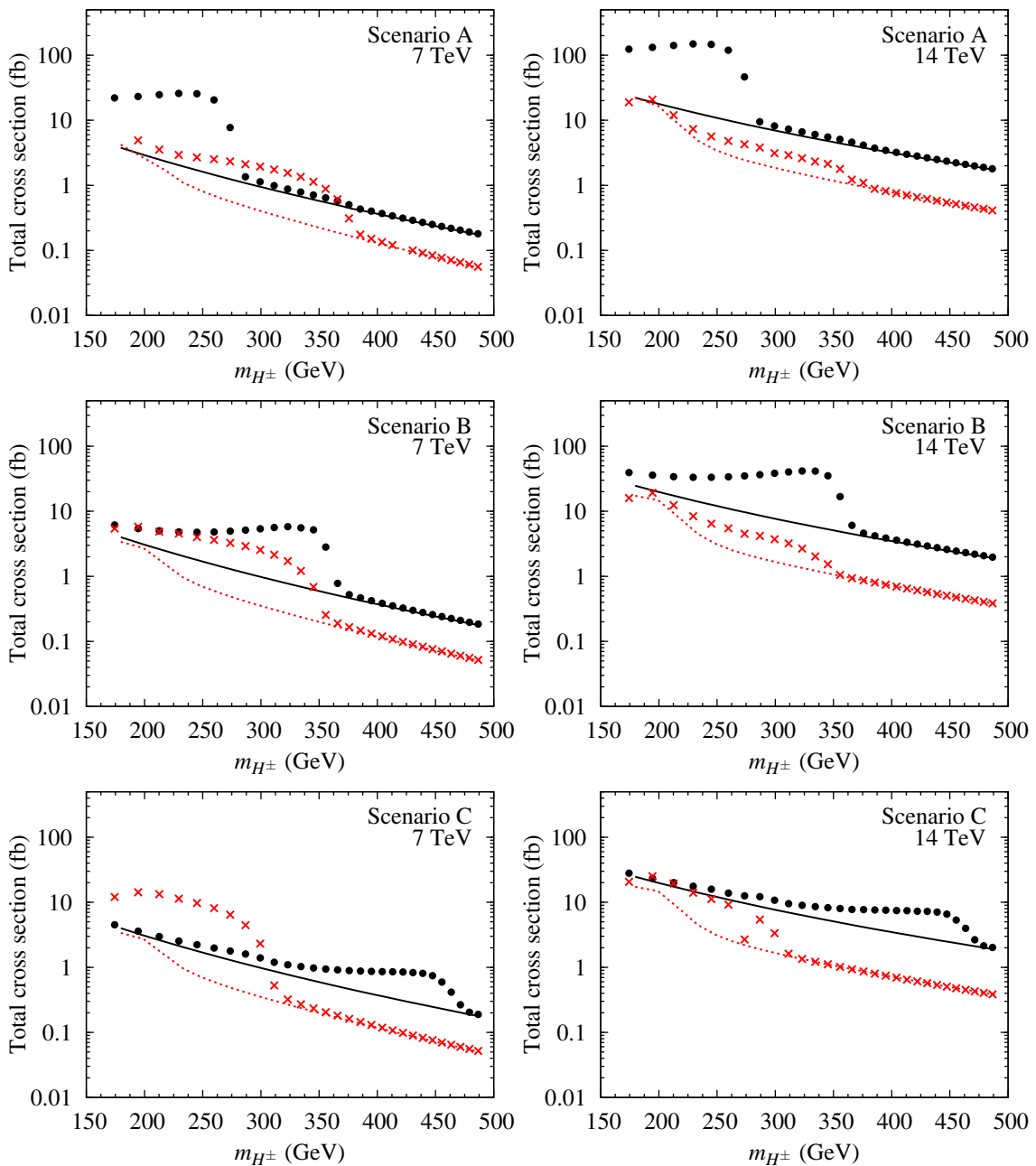


FIG. 9. Total hadronic cross section $pp \rightarrow H^\pm W^\mp$ at $\sqrt{s} = 7$ TeV (left) and $\sqrt{s} = 14$ TeV (right) as a function of the charged Higgs boson mass in scenarios A–C (with variable A_λ). The symbols indicate the separate contributions to the NMSSM cross section from $b\bar{b}$ (dots) and $g\bar{g}$ (crosses), while the lines show the corresponding contributions ($b\bar{b}$ solid, $g\bar{g}$ dotted) in the MSSM limit.

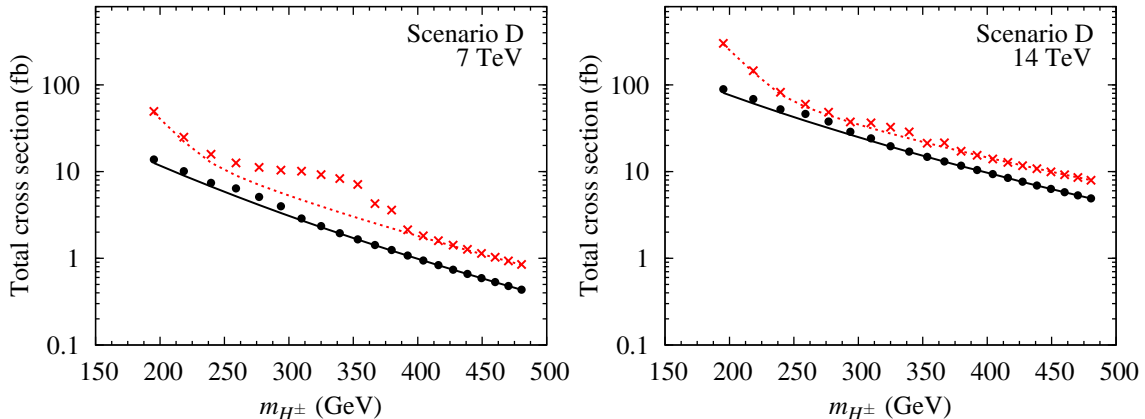


FIG. 10. Total hadronic cross section $pp \rightarrow H^\pm W^\mp$ at $\sqrt{s} = 7$ TeV (left) and $\sqrt{s} = 14$ TeV (right) for NMSSM Scenario D. The different symbols used are explained in the caption of Figure 9.

parton distributions [60] and a fixed $\mu_F = m_{H^\pm} + m_W$. The results for Scenarios A–C are presented in Fig. 9, shown in parallel for 7 TeV (left) and 14 TeV (right). We give the contributions of $b\bar{b}$ (big dots) and gg (crosses) separately, together with their respective contributions in the MSSM limit (as solid and dotted lines, respectively). By comparing the NMSSM results to the MSSM limit, it can be seen from these plots that it is possible to have substantial NMSSM enhancements also in the hadron-level cross section. In some mass ranges this enhancement can be an order of magnitude. The observed shapes, with an almost flat dependence of the cross section on the charged Higgs mass up to some mass, and then a rapid fall-off to the MSSM value, is caused by the contribution of the resonances. In the region where the $H^\pm W^\mp$ threshold is below the resonance mass (cf. Fig. 8), the cross section is dominated by the contribution of resonant diagrams. When the transition takes place, the non-resonant behavior quickly becomes similar to the MSSM case. Note that the contributions from $b\bar{b}$ and gg in general receive their largest resonant enhancements from two different resonances, as discussed in Section IV B. This also leads to the two different m_{H^\pm} regions where the cross section is flat for the two cases. Similarly to the discussion of the partonic cross sections above, we can see how the three scenarios A–C differ mainly in the position of the resonances, which results in a cross section enhancement (for $b\bar{b}$) at low m_{H^\pm} in Scenario A, and towards higher masses in Scenario C. The opposite is true for the gg contribution.

In Fig. 10 we show the hadronic cross section for Scenario D. We see from this figure that the low value of $\tan\beta$ in this scenario gives a significantly larger gg contribution to the total cross section than in the other cases; it dominates over $b\bar{b}$ for the full range of m_{H^\pm} . There is more room for a large gg contribution in the NMSSM, since lower $\tan\beta$ is still allowed in this model compared to the MSSM. We note a relatively small resonance enhancement in this scenario, in particular for $b\bar{b}$ where it is barely visible. For our last scenario, Scenario E, the cross section is shown in Fig. 11. With a large $\tan\beta$, this scenario has been selected to maximize the Higgs couplings to $b\bar{b}$, and indeed we find the largest total cross section for this scenario. As could be expected, the $b\bar{b}$ contribution dominates completely, being almost two orders of magnitude larger than gg for $m_{H^\pm} > 400$ GeV. In this scenario the resonances are again pronounced, and we observe clearly the coupling of $b\bar{b}$ to the (lighter) A_2 , while the gg contribution is more efficiently enhanced by the (heavier) H_3 resonance.

It is interesting to note from the hadron-level results that the relative importance of $b\bar{b}$

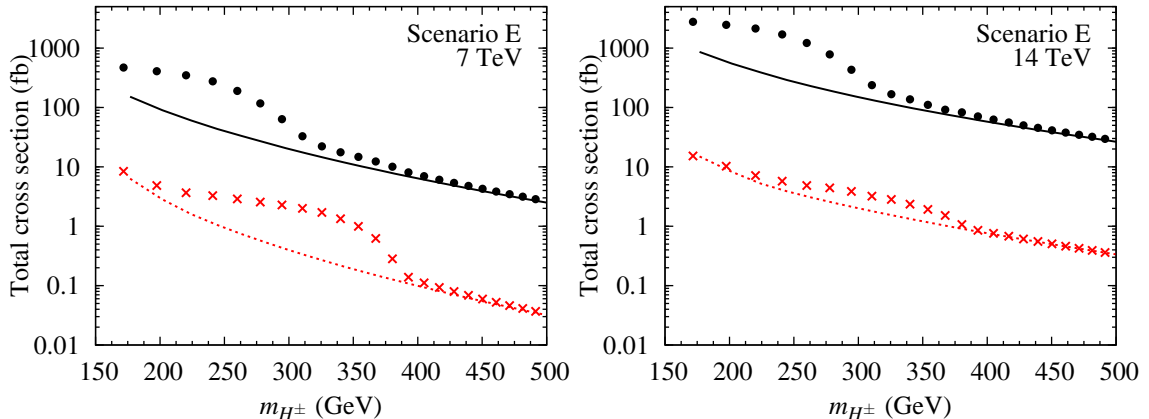


FIG. 11. Total hadronic cross section $pp \rightarrow H^\pm W^\mp$ at $\sqrt{s} = 7$ TeV (left) and $\sqrt{s} = 14$ TeV (right) for NMSSM Scenario E. The different symbols used are explained in the caption of Figure 9.

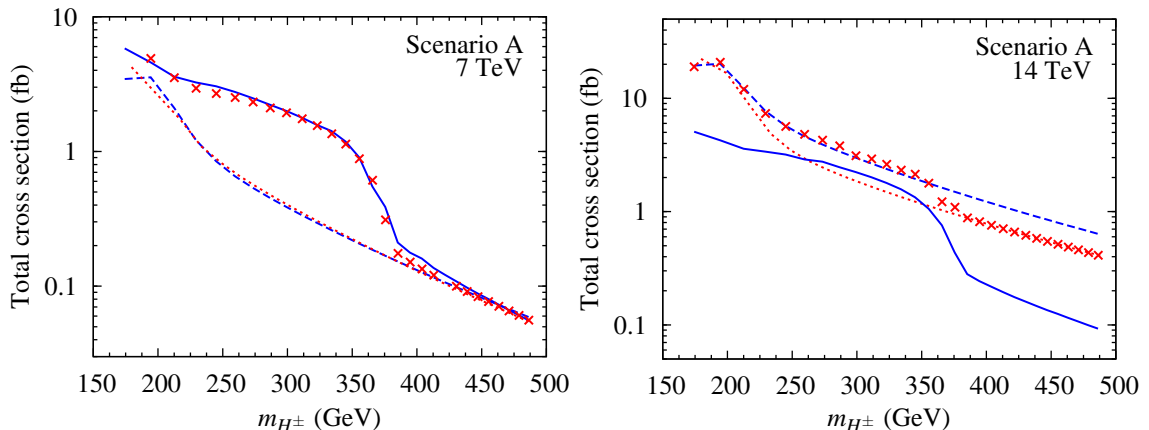


FIG. 12. The gluonic contribution to the total hadronic cross section $pp \rightarrow H^\pm W^\mp$ at $\sqrt{s} = 7$ TeV (left) and $\sqrt{s} = 14$ TeV (right) for NMSSM Scenario A (crosses) compared to the MSSM limit (dotted line). The blue lines correspond to the separate contributions to $gg \rightarrow H^\pm W^\mp$ from only including triangles (solid line) and box diagrams (dashed).

and gg may change drastically in regions where either of the resonances dominate. This change in the relative contributions can be much larger than what is expected from the energy scaling of the parton luminosities, cf. Fig. 7. It is a result of the different couplings of the H_3 and A_2 resonances to the initial and final states. In some of our scenarios the gg contribution can even become larger than the $b\bar{b}$ contribution in certain regions of m_{H^\pm} (in Scenario D, the neutral Higgses have a reduced coupling to b quarks, and the gg contribution is dominant for all values of m_{H^\pm}).

Another feature of the gg contribution to the hadronic cross section which deserves a comment is the apparent larger NMSSM enhancement at the 7 TeV LHC compared to the 14 TeV case. The shape of the enhancements is due to a convolution of the resonance peaks observed in the parton-level cross section with the dependence of the PDFs on the partonic center-of-mass energy $\sqrt{\hat{s}}$ (including the $x_{1,2}$ -dependence of the PDFs). There can also be interference effects between the resonant contributions and (non-resonant) boxes. To investigate the relative importance of the different contributions in some more detail, we

illustrate in Fig. 12 the contributions from (boxes)² and (triangles)² to the total cross section for Scenario A. At $\sqrt{s} = 7$ TeV, we see that the box and triangle contributions are similar in the non-resonant region, i.e. at relatively large charged Higgs masses $m_{H^\pm} \gtrsim 380$ GeV. Interestingly enough, the full cross section is numerically at the same level as separately the box and triangle contributions, which means that the destructive interference between the two is large and similar to that in MSSM. However, in the resonant region (corresponding to $m_{H^\pm} < 380$ GeV), the triangle contribution becomes much more pronounced and strongly enhances the total cross section. The interference effects are naturally quite small there. At higher energies, $\sqrt{s} = 14$ TeV, we observe a somewhat different picture in Fig. 12. The boxes in this case gives a large (dominant) contribution to the total gluon-initiated cross section over the whole range in m_{H^\pm} . In the non-resonant region, $m_{H^\pm} \gtrsim 380$ GeV, the interference with the smaller triangle contribution noticeably decreases the cross section compared to the box contribution alone. In the resonant region, $m_{H^\pm} < 380$ GeV, the triangles become more important, but remain sub-dominant compared to the boxes. The cross section is therefore only enhanced slightly with respect to the MSSM case. Analogously to the 7 TeV case, the interference turns out to be less important than in the non-resonant region.

V. COLLIDER PHENOMENOLOGY

We have shown that the total cross sections for associated $H^\pm W^\mp$ production in the NMSSM can be substantially enhanced compared to the corresponding cross sections in the MSSM. We would now like to discuss the phenomenological implications of this for searches at the LHC. Dedicated collider studies of this channel have been performed for MSSM and two-Higgs doublet models [22, 25–28]. While we will comment here on what features of these studies that are relevant for NMSSM—and what features will be different—we leave a dedicated phenomenological study for the future, since this would require calculation of differential cross sections and consideration of backgrounds and sensitivities.

The defining feature of the various possible ways of detecting associated production is how the charged Higgs decays. The previous studies have all concentrated on the decays that are relevant in the MSSM or 2HDM, namely $H^+ \rightarrow \tau^+ \nu, c\bar{s}$ for light charged Higgs bosons and $H^+ \rightarrow t\bar{b}$ for heavy charged Higgs. Decays to SUSY particles may also be important for heavy H^\pm . As we discussed above, in the NMSSM the decay $H^\pm \rightarrow W^\pm A_1$ is sometimes dominant, and will lead to quite different experimental requirements. This channel is normally not possible in the MSSM, since m_A and m_{H^\pm} are close to degenerate. In the NMSSM, the decay width is proportional to the doublet component of A_1 , but may be large even if the A_1 is mostly singlet [10, 11]. The A_1 boson can be very light in the NMSSM, and in such a case its dominant decays will be $A_1 \rightarrow b\bar{b}$ or $A_1 \rightarrow \tau^+ \tau^-$. We do not consider scenarios with a light A_1 in this paper, but they could nevertheless be of interest.

In Fig. 13 we show the decay branching ratios of H^+ , calculated using NMSSMTOOLS, for three of our benchmark scenarios. Since the most important parameter entering the determination of the decay modes is $\tan\beta$, the results for scenarios B and C are very similar to those for Scenario A and we do not show them explicitly. All our scenarios have, as explained above, charged Higgs masses above the threshold for the decay $H^+ \rightarrow t\bar{b}$. As can be seen from Fig. 13, the decay $H^+ \rightarrow t\bar{b}$ dominates over a wide range in masses, but for scenarios A and E the decay $H^+ \rightarrow \tau^+ \nu$ is appreciable over the entire mass ranges plotted, and dominates close to the $t\bar{b}$ threshold. The $H^\pm \rightarrow W^\pm A_1$ decay is only relevant for Scenario D, which has a somewhat lighter A_1 , or for very heavy H^+ in scenarios A–C. SUSY

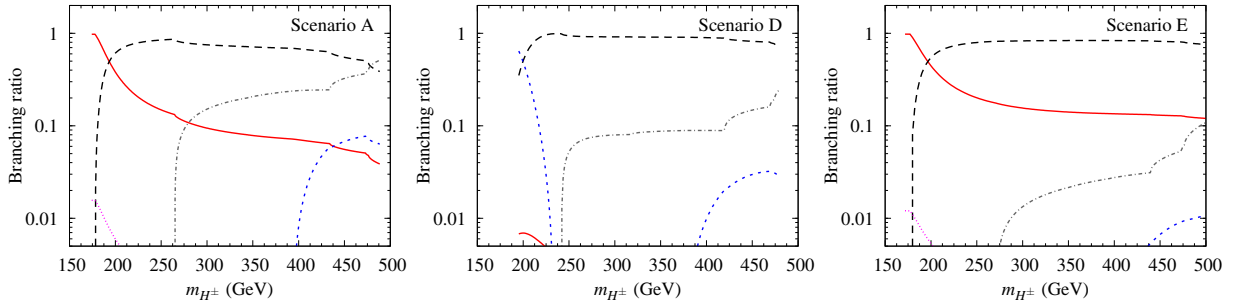


FIG. 13. Charged Higgs branching ratios $H^+ \rightarrow \tau^+\nu$ (solid, red), $H^+ \rightarrow t\bar{b}$ (long dashes, black), $H^+ \rightarrow c\bar{b}$ (dotted, purple), $H^+ \rightarrow W^+A_1$ (short dashes, blue), and $H^+ \rightarrow \text{SUSY}$ (dot-dashed, gray) for NMSSM benchmark scenarios A (left), D (center), and E (right).

decays to a chargino-neutralino pair, $H^+ \rightarrow \tilde{\chi}_1^+ \tilde{\chi}_1^0$, also become appreciable above threshold, but this of course depends very much on the parameters entering the neutralino and chargino sectors. To summarize, the situation for our scenarios is thus similar to the MSSM case in terms of decay channels, except possibly for Scenario D. However, the possible Higgs masses and the size of the cross sections can be different. We also would like to emphasize that, for a complete coverage of the phenomenological possibilities in the NMSSM, other scenarios where the decay modes are different should be considered.

Previous collider studies, which were all based on the MSSM, have thus used either the $H^+ \rightarrow \tau^+\nu$ or the $H^+ \rightarrow t\bar{b}$ decay channels. We will now make some simple estimates of how these results translate to the NMSSM. Keep in mind that although we can draw some general conclusions based on these estimates, there may be more subtle differences, caused e.g. by different dependences of the differential cross sections on kinematical variables when the relative contributions of different types of processes are different.

In [26], the $H^+ \rightarrow \tau^+\nu$ channel was considered with hadronic τ and W^\mp decays. The main background to this signal is the production of $W + 2$ jets. A parton-level study showed that for $m_{H^\pm} = 175$ GeV in the m_h^{max} scenario at $\tan\beta = 50$, it should be possible after a series of cuts to get a statistically significant signal at the 14 TeV LHC with 300 fb^{-1} of data. In this scenario, the total production cross section was 55 fb, with a charged Higgs branching ratio into $\tau^+\nu$ of 100%, and the obtained S/\sqrt{B} value was 17. We may rescale this result to e.g. our Scenario A (with a much lower $\tan\beta$), where the cross section is, conservatively, 100 fb and the branching ratio $\text{BR}(H^+ \rightarrow \tau^+\nu) = 100\%$, which would yield a significance of about $S/\sqrt{B} = 30$. A scenario with $m_{H^\pm} = 400$ GeV was also studied [26], but here the significance was only $S/\sqrt{B} = 2.6$ due to the lower cross section and branching ratio. At this higher mass, we do not predict an enhancement of the cross section in the NMSSM for Scenario A, but rather a similar cross section to the one in the MSSM; our expected significance should therefore be similar. If we instead consider Scenario C, which has the resonant enhancement at a higher mass, the cross section at $m_{H^\pm} = 400$ GeV is 10 fb, while the branching ratio is about 10% (instead of 20%). This would yield a higher significance, but still not above $S/\sqrt{B} = 5$. Similar conclusions as those presented in [26] were found in [22], and more recently in [27], where a detailed study of discovery contours in the MSSM was performed using both leptonic and hadronic W decays.

The $H^+ \rightarrow t\bar{b}$ decay was first studied in [25], where hadronic decays of the top quark and the W from the top quark, and leptonic decay of the other W were considered. The hadronic decay of the H^\pm has the advantage over the $\tau\nu$ channel that the mass can be completely

reconstructed, while the charged lepton from the other W provides a useful trigger. The conclusion of this work was unfortunately that the $t\bar{t}$ background completely overwhelms the signal. However, it was recently argued [28] that with the use of optimized cuts this channel can be useful to obtain significant results. No numbers for the significance of the $H^+ \rightarrow t\bar{b}$ channel have been given in [25], but we note that in our Scenario A, the total cross section times branching ratio at $m_{H^\pm} = 200$ GeV is roughly 10 times larger than the one used in the analysis there, and it is therefore plausible that the significance could be improved.

The remaining, possibly useful, decay channel is $H^\pm \rightarrow W^\pm A_1$, followed by $A_1 \rightarrow b\bar{b}$ or $A_1 \rightarrow \tau^+\tau^-$ decay. Note that the final state in the $b\bar{b}$ case is the same as for the hadronic $H^+ \rightarrow t\bar{b}$ case, but with a $b\bar{b}$ pair that should reconstruct the A_1 mass. This may provide an additional handle on the signal, but it is not obvious that this is useful experimentally; it may be that the $\tau^+\tau^-$ decay proves more useful. If possible, we would like to suggest to the experiments that $t\bar{t}$ samples with leptonic W decays are investigated for $b\bar{b}$ resonances. To look for (low mass) $b\bar{b}$ resonances in more energetic events has also been proposed recently as a means of searching for light, singlet-dominated, NMSSM Higgs bosons produced in SUSY cascades [61]. In any case, we think that the $H^\pm \rightarrow W^\pm A_1$ channel deserves a detailed study, and as far as we know this has not been performed for the case of $H^\pm W^\mp$ production.

VI. SUMMARY AND CONCLUSIONS

We have studied associated charged Higgs and W boson production in the NMSSM. This process is complementary to the main production modes anticipated for heavy charged Higgs bosons ($m_{H^\pm} > m_t$) at the LHC. We calculated the leading order contributions to the total hadronic cross section $pp \rightarrow H^\pm W^\mp$ in a general NMSSM setting, corresponding to the tree-level $b\bar{b}$ contribution and the gg -initiated subprocess at one loop. The calculation has been performed using an improved Born approximation, taking into account the most important effects of (S)QCD higher order corrections.

For $H^\pm W^\mp$ production in the NMSSM, we have first investigated the parameter dependence of the parton-level cross section and the corresponding result in the MSSM limit. Starting from a maximal mixing scenario, we have then defined five NMSSM benchmark scenarios, with the common feature that they allow for resonant contributions from heavy singlet-like Higgs bosons. These resonances couple both to the $b\bar{b}$ and gg initial states, and we find that they can lead to significant enhancements of the cross section (by up to an order of magnitude) over a wide range of charged Higgs masses in the benchmark scenarios. The presence of these resonances is a genuine feature of the NMSSM, since Higgs mass configurations like this are not possible in the MSSM. This process might therefore be useful as a discriminator between the two models.

We also discussed briefly the phenomenological implications of $H^\pm W^\mp$ production in the NMSSM. Based on previous work for the MSSM, we estimated the discovery significance that could be expected for different decay channels of H^\pm . From these estimates it seems likely that the chances of detecting the charged Higgs boson of the NMSSM at the LHC through this process are quite good, at least in scenarios similar to ours with a not too heavy H^\pm . It may not even be necessary to wait for the 300 fb $^{-1}$ at 14 TeV that were previously assumed in MSSM studies, but clearly it will still require more data than “standard” Higgs searches. However, it should be remembered that these results are rough estimates based on rescaling of earlier MSSM results with the total cross section ratio. More detailed Monte

Carlo studies should therefore be done, for example on the impact of the different kinematics between the resonant and non-resonant contributions. It would also be necessary to revise previous results for the present and future running conditions of the LHC, something which is also true for the existing MSSM studies. To more seriously assess the prospects of observing associated $H^\pm W^\mp$ production at the LHC it would eventually be necessary to perform an analysis at the level of full experimental detector simulation. Perhaps the encouragement provided by these positive results could trigger the interest necessary to revisit this channel as a probe for the NMSSM and other models beyond the MSSM.

ACKNOWLEDGMENTS

Helpful discussions with Johan Rathsman are gratefully acknowledged. R.E. was supported by the Swedish Research Council under contract 2007-4071. R.P. was supported by the Carl Trygger Foundation (Sweden). O.S. was supported by the Collaborative Research Center SFB676 of the DFG, “Particles, Strings, and the Early Universe”.

-
- [1] H. P. Nilles, *Phys. Rept.* **110**, 1 (1984).
 - [2] H. E. Haber and G. L. Kane, *Phys. Rept.* **117**, 75 (1985).
 - [3] R. Barbieri, L. J. Hall, Y. Nomura, and V. S. Rychkov, *Phys. Rev. D* **75**, 035007 (2007), hep-ph/0607332.
 - [4] L. J. Hall, D. Pinner, and J. T. Ruderman (2011), 1112.2703.
 - [5] U. Ellwanger, C. Hugonie, and A. M. Teixeira, *Phys. Rept.* **496**, 1 (2010), 0910.1785.
 - [6] M. Maniatis, *Int. J. Mod. Phys. A* **25**, 3505 (2010), 0906.0777.
 - [7] P. Draper, T. Liu, C. E. Wagner, L.-T. Wang, and H. Zhang, *Phys. Rev. Lett.* **106**, 121805 (2011), 1009.3963.
 - [8] D. A. Vasquez, G. Belanger, C. Boehm, A. Pukhov, and J. Silk, *Phys. Rev. D* **82**, 115027 (2010), 1009.4380.
 - [9] R. Dermisek and J. F. Gunion, *Phys. Rev. Lett.* **95**, 041801 (2005), hep-ph/0502105.
 - [10] A. Akeroyd, A. Arhrib, and Q.-S. Yan, *Eur. Phys. J. C* **55**, 653 (2008), 0712.3933.
 - [11] F. Mahmoudi, J. Rathsman, O. Stål, and L. Zeune, *Eur. Phys. J. C* **71**, 1608 (2011), 1012.4490.
 - [12] R. Enberg and R. Pasechnik, *Phys. Rev. D* **83**, 095020 (2011), 1104.0889.
 - [13] D. Dicus, J. Hewett, C. Kao, and T. Rizzo, *Phys. Rev. D* **40**, 787 (1989).
 - [14] A. Barrientos Bendezu and B. A. Kniehl, *Phys. Rev. D* **59**, 015009 (1999), hep-ph/9807480.
 - [15] A. Barrientos Bendezu and B. A. Kniehl, *Phys. Rev. D* **61**, 097701 (2000), hep-ph/9909502.
 - [16] A. Barrientos Bendezu and B. A. Kniehl, *Phys. Rev. D* **63**, 015009 (2001), hep-ph/0007336.
 - [17] O. Brein, W. Hollik, and S. Kanemura, *Phys. Rev. D* **63**, 095001 (2001), hep-ph/0008308.
 - [18] E. Asakawa, O. Brein, and S. Kanemura, *Phys. Rev. D* **72**, 055017 (2005), hep-ph/0506249.
 - [19] Y.-S. Yang, C.-S. Li, L.-G. Jin, and S. H. Zhu, *Phys. Rev. D* **62**, 095012 (2000), hep-ph/0004248.
 - [20] W. Hollik and S.-h. Zhu, *Phys. Rev. D* **65**, 075015 (2002), hep-ph/0109103.
 - [21] J. Zhao, C. S. Li, and Q. Li, *Phys. Rev. D* **72**, 114008 (2005), hep-ph/0509369.
 - [22] J. Gao, C. S. Li, and Z. Li, *Phys. Rev. D* **77**, 014032 (2008), 0710.0826.
 - [23] M. Rauch (2008), Ph.D. Thesis, 0804.2428.
 - [24] T. N. Dao, W. Hollik, and D. N. Le, *Phys. Rev. D* **83**, 075003 (2011), 1011.4820.

- [25] S. Moretti and K. Odagiri, *Phys. Rev. D* **59**, 055008 (1999), hep-ph/9809244.
- [26] D. Eriksson, S. Hesselbach, and J. Rathsman, *Eur. Phys. J. C* **53**, 267 (2008), hep-ph/0612198.
- [27] M. Hashemi, *Phys. Rev. D* **83**, 055004 (2011), 1008.3785.
- [28] S.-S. Bao, X. Gong, H.-L. Li, S.-Y. Li, and Z.-G. Si (2011), 1112.0086.
- [29] The ATLAS Collaboration (2011), ATLAS-CONF-2011-138.
- [30] The ATLAS Collaboration (2011), ATLAS-CONF-2011-151.
- [31] The CMS Collaboration (2011), CMS PAS HIG-11-008.
- [32] R. Dermisek and J. F. Gunion, *Phys. Rev. D* **79**, 055014 (2009), 0811.3537.
- [33] R. Dermisek and J. F. Gunion, *Phys. Rev. D* **81**, 055001 (2010), 0911.2460.
- [34] R. Dermisek and J. F. Gunion, *Phys. Rev. D* **81**, 075003 (2010), 1002.1971.
- [35] U. Ellwanger, *Phys. Lett. B* **303**, 271 (1993), hep-ph/9302224.
- [36] T. Elliott, S. King, and P. White, *Phys. Lett. B* **305**, 71 (1993), hep-ph/9302202.
- [37] T. Elliott, S. King, and P. White, *Phys. Lett. B* **314**, 56 (1993), hep-ph/9305282.
- [38] T. Elliott, S. King, and P. White, *Phys. Rev. D* **49**, 2435 (1994), hep-ph/9308309.
- [39] P. Pandita, *Phys. Lett. B* **318**, 338 (1993).
- [40] U. Ellwanger and C. Hugonie, *Phys. Lett. B* **623**, 93 (2005), hep-ph/0504269.
- [41] F. Staub, W. Porod, and B. Herrmann, *JHEP* **1010**, 040 (2010), 1007.4049.
- [42] K. Ender, T. Graf, M. Muhlleitner, and H. Rzehak (2011), 1111.4952.
- [43] G. Degrossi and P. Slavich, *Nucl. Phys. B* **825**, 119 (2010), 0907.4682.
- [44] U. Ellwanger, J. F. Gunion, and C. Hugonie, *JHEP* **02**, 066 (2005), hep-ph/0406215.
- [45] U. Ellwanger and C. Hugonie, *Comput. Phys. Commun.* **175**, 290 (2006), hep-ph/0508022.
- [46] M. S. Carena, S. Heinemeyer, C. E. M. Wagner, and G. Weiglein (1999), hep-ph/9912223.
- [47] M. S. Carena, S. Heinemeyer, C. E. M. Wagner, and G. Weiglein, *Eur. Phys. J. C* **26**, 601 (2003), hep-ph/0202167.
- [48] A. Pilaftsis, *Nucl. Phys. B* **504**, 61 (1997), hep-ph/9702393.
- [49] J. R. Ellis, J. S. Lee, and A. Pilaftsis, *Phys. Rev. D* **70**, 075010 (2004), hep-ph/0404167.
- [50] L. Avdeev and M. Kalmykov, *Nucl. Phys. B* **502**, 419 (1997), hep-ph/9701308.
- [51] L. J. Hall, R. Rattazzi, and U. Sarid, *Phys. Rev. D* **50**, 7048 (1994), hep-ph/9306309.
- [52] M. S. Carena, S. Mrenna, and C. Wagner, *Phys. Rev. D* **60**, 075010 (1999), hep-ph/9808312.
- [53] M. S. Carena, D. Garcia, U. Nierste, and C. E. M. Wagner, *Nucl. Phys. B* **577**, 88 (2000), hep-ph/9912516.
- [54] T. Hahn and C. Schappacher, *Comput. Phys. Commun.* **143**, 54 (2002), hep-ph/0105349.
- [55] T. Hahn, *Comput. Phys. Commun.* **140**, 418 (2001), hep-ph/0012260.
- [56] T. Hahn and M. Perez-Victoria, *Comput. Phys. Commun.* **118**, 153 (1999), hep-ph/9807565.
- [57] R. Barate et al. (LEP Working Group for Higgs boson searches), *Phys. Lett. B* **565**, 61 (2003), hep-ex/0306033.
- [58] P. Bechtle, O. Brein, S. Heinemeyer, G. Weiglein, and K. E. Williams, *Comput. Phys. Commun.* **182**, 2605 (2011), 1102.1898.
- [59] A. D. Martin, W. J. Stirling, R. S. Thorne, and G. Watt, *Eur. Phys. J. C* **63**, 189 (2009), 0901.0002.
- [60] P. M. Nadolsky et al., *Phys. Rev. D* **78**, 013004 (2008), 0802.0007.
- [61] O. Stål and G. Weiglein (2011), 1108.0595.